Journal of Wind Engineering & Industrial Aerodynamics 174 (2018) 69–79

Contents lists available at ScienceDirect

Journal of Wind Engineering & Industrial Aerodynamics

journal homepage: www.elsevier.com/locate/jweia

Prediction of frequency distribution of strong crosswind in a control section for train operations by using onsite measurement and numerical simulation

Yayoi Misu [a,*], Takeshi Ishihara [b]

[a] Safety Research Lab, R&D Center of JR East Group, East Japan Railway Company, Japan
[b] Department of Civil Engineering, School of Engineering, The University of Tokyo, Japan

ARTICLE INFO

Keywords:
Frequency distribution of strong crosswind
Onsite measurement
Numerical simulation
Control section
Regulation of train operation

ABSTRACT

In this study, a prediction method for strong wind using onsite measurement and numerical simulation is used to take account of the effects of complex terrain. The predicted maximum winds agree well with the measurements. A time series based method is proposed to predict the frequency of exceedance of strong crosswind in a control section. The predicted frequency of exceedance of strong crosswind agrees well with the measurements, while conventional methods based on only statistical data underestimate or overestimate the frequency. The proposed method is applied in order to estimate the regulation frequency in train operation, considering train speed, wind direction, and windbreaks. The regulation frequency at a target control section of 6 km decreases from 0.16% to 0.14% when the train speed is reduced. The frequency decreases from 0.16% to 0.11% if the wind direction is considered. The construction of the windbreaks decreases the frequency further to 0.08%.

1. Introduction

In railways, some accidents that lead to train turning over or derailment are caused by strong crosswinds, and the regulation of railway operation became stricter after these accidents were reported (Fujii et al., 1995). After obtaining the knowledge that the maximum instantaneous wind speed is highly dominant to the overturning of the train from a study of the accident in 1986 (Nakao), the regulation in Japan has subsequently been governed by the measured maximum instantaneous wind speed in a control section set within a continuous railway track. As Kunieda (1972) and Hibino et al. (2011). mentioned, critical wind speed of train overturning can be improved if the train speed is reduced. Therefore, the train speed is reduced or the train is stopped if measured or predicted wind speed in the control section exceeds a threshold set by a railway company considering the critical wind speed of train overturning. By this regulation, train delay time increases if the measured or predicted wind speed exceeds the threshold frequently. In order to reduce the duration of the regulation, Fujii (1998), Matsuda et al. (1997), and Imai et al. (2002). proposed regulation methods considering wind directions. Tanemoto et al. (2005), Avila-Sanches et al. (2014). studied the effect of windbreaks to reduce the side wind force induced on the train, and East Japan Railway Company introduced the windbreaks along the railway tracks (East Japan Railway Company, 2016). In order to realize efficient operation control under the strong wind, the effectiveness of countermeasures should be validated quantitatively by prediction for the frequency of exceedance of strong crosswind in the control section.

There are two methods to predict the frequency of exceedance of strong crosswind in the control section. In one method (Hibino et al., 2011), the frequency is predicted from wind speed measured by one anemometer installed in the control section, which is used by many railway companies especially in Japan. The frequency by this method can be estimated by only considering the measured wind speed. However, the frequency might be underestimated if the strongest wind does not brow at the measurement site. In another method proposed by Matschke et al. (2000). and Cleon et al. (Cléon et al., 2002), the control section is divided into number of sub-sections and the strong wind in each sub-section is predicted by a combination of measured wind speed and those obtained from numerical simulation. Although this method can take account of the winds which blows at sites where the anemometer is not installed, the frequency of strong crosswind might be overestimated because it is assumed that there is no correlation between the wind speeds in sub-sections.

In this study, a prediction method for maximum wind speed and direction at sites along a railway track is proposed by using onsite measurement and numerical simulation. The predicted maximum wind speed and direction by the proposed method are verified by measured those at the sites. Then, a new method is proposed to predict the frequency of exceedance of strong crosswinds in a control section with consideration

* Corresponding author.
E-mail address: y-misu@jreast.co.jp (Y. Misu).

https://doi.org/10.1016/j.jweia.2017.11.020
Received 9 March 2017; Received in revised form 3 May 2017; Accepted 20 November 2017

of the correlation between strong crosswinds at different sub-sections. The accuracy of the proposed method is evaluated and the disadvantage of the existing methods is clarified by comparison with the onsite measurement. Finally, the effect of countermeasures against the strong crosswind, such as reducing train speed, regulation considering wind directions, and installation of windbreaks, are assessed using the proposed method.

2. Strong wind prediction along a railway track

In this section, maximum wind speed and wind direction are predicted by a method using an onsite measurement and numerical simulation technique. In this method, the effects of local terrain on the wind speed and the wind direction are taken into account.

2.1. Prediction of maximum wind speed and wind direction

The wind speed ratio, S_{pr}, and change in wind direction, D_{pr}, between a reference site, where an anemometer is installed, and a prediction site, where wind speed and direction are to be estimated, are obtained from the numerical simulation. A time series of mean wind speed and wind direction at the prediction site, u_p and θ_p, are estimated by multiplying the wind speed ratio and adding the change in wind direction to a time series of measured mean wind speed, u_r, and wind direction, θ_r, at the reference site as:

$$u_p = u_r \times S_{pr} \tag{1}$$

$$\theta_p = \theta_r + D_{pr} \tag{2}$$

where subscripts p, r, and pr means the prediction site, the reference site, and the relationship between the prediction site and the reference site respectively. The maximum wind speed $\widehat{u}_p$ at the prediction site can be calculated by multiplying the gust factor G_p, defined by the ratio of the maximum to the mean speed, to the predicted mean wind speed u_p as:

$$\widehat{u}_p = u_p \times G_p = u_r \times S_{pr} \times G_p \tag{3}$$

Because wind directions of the maximum winds, $\widehat{\theta}_p$, are consistent with the wind directions of the mean winds (Misu and Ishihara, 2012), it can be approximated by

$$\widehat{\theta}_p \cong \theta_p \tag{4}$$

The gust factor G_p can be estimated using the peak factor k_p, which is defined by the ratio of the maximum to the standard deviation of fluctuating wind speed and proposed by Ishizaki (1983), and the turbulence intensity I_p, which is obtained by a microscale wind prediction model (Yamaguchi et al., 2003; Ishihara and Hibi, 2002), as follows:

$$G_p = 1 + k_p I_p \tag{5}$$

$$k_p = \frac{1}{2}\ln\frac{T}{t} \tag{6}$$

where T is a reference time and t is an averaging time. In this study, the reference time is 60 s and the averaging time is three seconds.

The flow chart of the proposed method is shown in Fig. 1.

2.2. Prediction of wind speed and wind direction by numerical simulation

The microscale wind climates in a target domain can be predicted using a numerical simulation (Yamaguchi et al., 2003; Ishihara and Hibi, 2002; Liu et al., 2016a, 2016b). The governing equations of this model in this study, equations of continuity and momentum conservation, are as follows:

$$\frac{\partial \rho \overline{u}_j}{\partial x_j} = 0 \tag{7}$$

$$\frac{\partial \rho \overline{u}_i}{\partial t} + \frac{\partial \rho \overline{u}_j \overline{u}_i}{\partial x_j} = -\frac{\partial \overline{p}}{\partial x_i} + \frac{\partial}{\partial x_j}\left(\mu \frac{\partial \overline{u}_i}{\partial x_j} - \rho \overline{u_i' u_j'}\right) \tag{8}$$

where $\overline{u}_i$ and u'_i are average wind speed and fluctuating wind speed in x_i direction. ρ is density, $\overline{p}$ is average pressure, and μ is viscosity of fluid.

Reynolds stress $-\rho \overline{u_i' u_j'}$ can be approximated by a linear eddy viscosity model as:

$$\rho \overline{u_i' u_j'} = \frac{2}{3}\rho k \delta_{ij} - \mu_t\left(\frac{\partial u_i}{\partial x_j} + \frac{\partial u_j}{\partial x_i}\right) \tag{9}$$

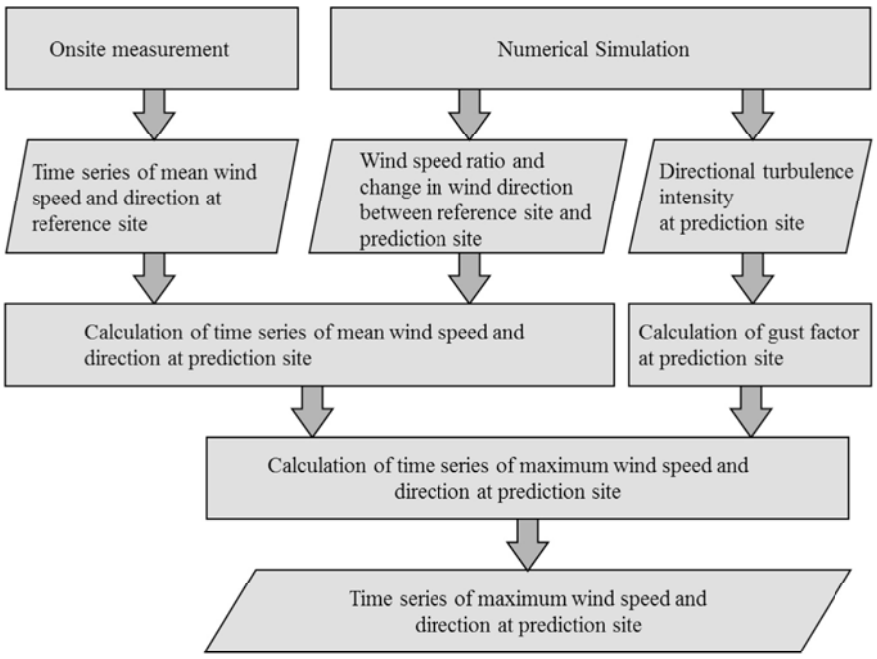

Fig. 1. Flow chart of prediction method for strong wind using onsite measurement and numerical simulation.

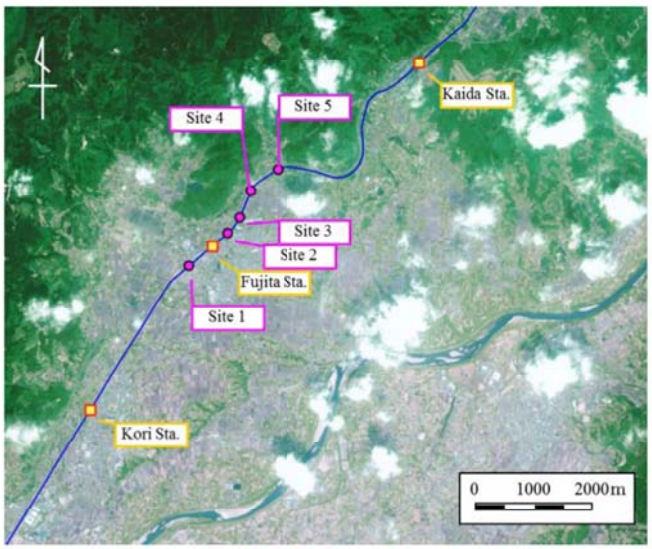

Fig. 2. Terrain around target area includes a train track between Kori and Kaida stations on Tohoku line.

In this study, a standard k-ε model is used. Turbulent energy, k, and rate of turbulent energy dissipation, ε, are obtained by following advection equations:

$$\frac{\partial \rho k}{\partial t} + \frac{\partial \rho \overline{u}_j k}{\partial x_j} = \frac{\partial}{\partial x_j}\left[\left(\mu + \frac{\mu_t}{\sigma_k}\right)\frac{\partial k}{\partial x_j}\right] - \rho\overline{u_i' u_j'}\frac{\partial \overline{u}_i}{\partial x_j} - \rho\varepsilon \tag{10}$$

$$\frac{\partial \rho \varepsilon}{\partial t} + \frac{\partial \rho \overline{u}_j \varepsilon}{\partial x_j} = \frac{\partial}{\partial x_j}\left[\left(\mu + \frac{\mu_t}{\sigma_\varepsilon}\right)\frac{\partial \varepsilon}{\partial x_j}\right] - C_{\varepsilon 1}\frac{\varepsilon}{k}\rho\overline{u_i' u_j'}\frac{\partial \overline{u}_i}{\partial x_j} - C_{\varepsilon 2}\frac{\rho\varepsilon^2}{k} \tag{11}$$

where μ_t is turbulent viscosity obtained by

$$\mu_t = C_\mu \rho \frac{k^2}{\varepsilon} \tag{12}$$

and the parameters in the standard k-ε model are $C_\mu = 0.09$, $\sigma_k = 1.0$, $\sigma_\varepsilon = 1.3$, $C_{\varepsilon 1} = 1.44$, and $C_{\varepsilon 2} = 1.92$.

In this study, an area including a train track between Kori station and Kaida station of Tohoku line as shown in Fig. 2 is used as a target domain. Wind measurements from site 1 to site 5 shown in Fig. 2 were conducted for one year from Feb. 2004 to Jan. 2005. The target domain which is a square having a center at site 3 with a side 7 km is set inside a circumscribed circle inscribed in an analytical domain as shown in Fig. 3. An additional domain which has the same area of the analytical domain is also set at the upwind region to consider the influence of upwind terrain and buffer zones are laid all around these domains, following the method proposed by Ishihara et al. (2003). Finer meshes are used at a nest domain inside the target domain to improve the accuracy of calculation. Detailed information of the grid system in the computational domains are shown in Table 1.

Fig. 4 shows terrain information in the nesting domain of the target

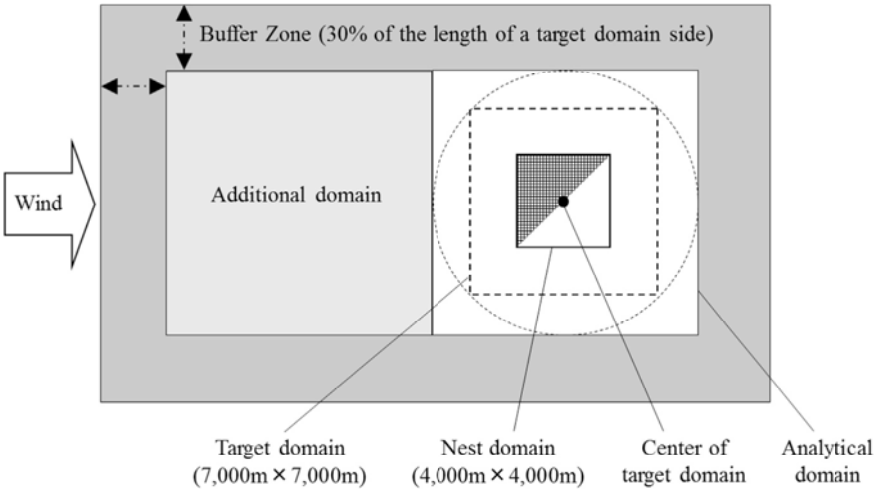

Fig. 3. Computational domains.

Table 1
Grid system and computational domains.

Latitude/Longitude of the target domain center			N3753′02.3″ E14032′42.8″
Number of wind direction sectors			32 (11.25° each)
Land use information (Terrain roughness)			1/10 land use raster data (100 m mesh) Published by Geospatial Information Authority of Japan
Target domain	Area	X × Y × Z	7,000m × 7,000m × 1,500 m
	Grid size	Horizontal X,Y	40 m-200 m
		Vertical Z	5 m
	Stretching ratio	X, Y, Z	1.1 times
	The number of grids (X × Y × Z)		228 × 178 × 41 (=1,663,944)
	Information of altitude		Digital map (50 m) Published by Geospatial Information Authority of Japan
Nesting domain	Area	X × Y × Z	4,000m × 4,000m × 1,500 m
	Minimum interval of mesh	Horizontal X,Y	20 m
		Vertical Z	5 m
	Stretching ratio	Horizontal X,Y	1.0 times
		Vertical Z	1.1 times
	The number of grids (X × Y × Z)		202 × 202 × 41 (=1,672,964)
	Information of altitude		GISMAP Terrain (10 m) Published by Hokkaido Chizu Corporation

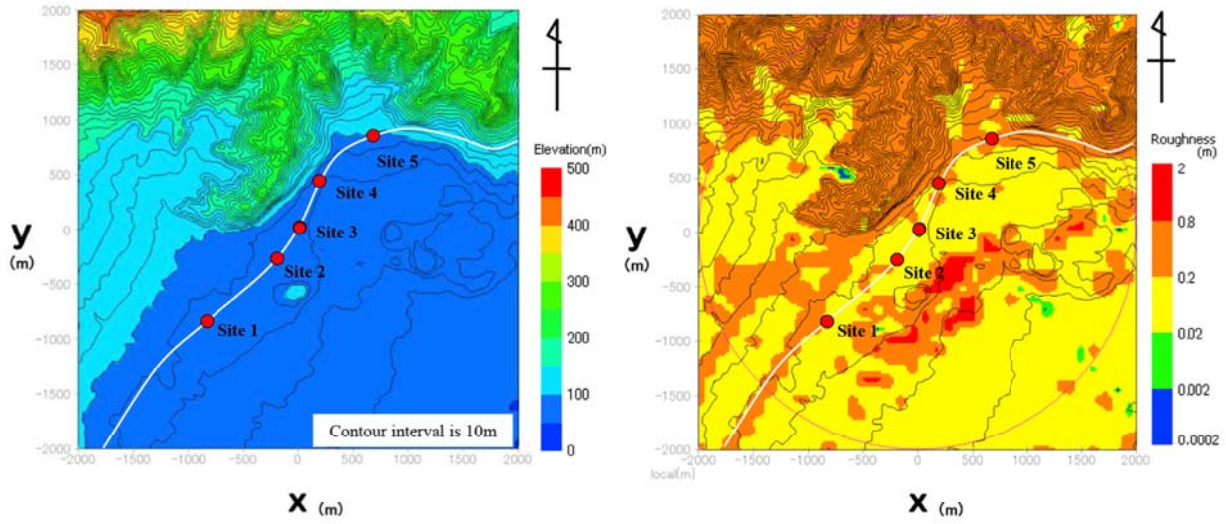

Fig. 4. Elevation contour and surface roughness around the target control section.

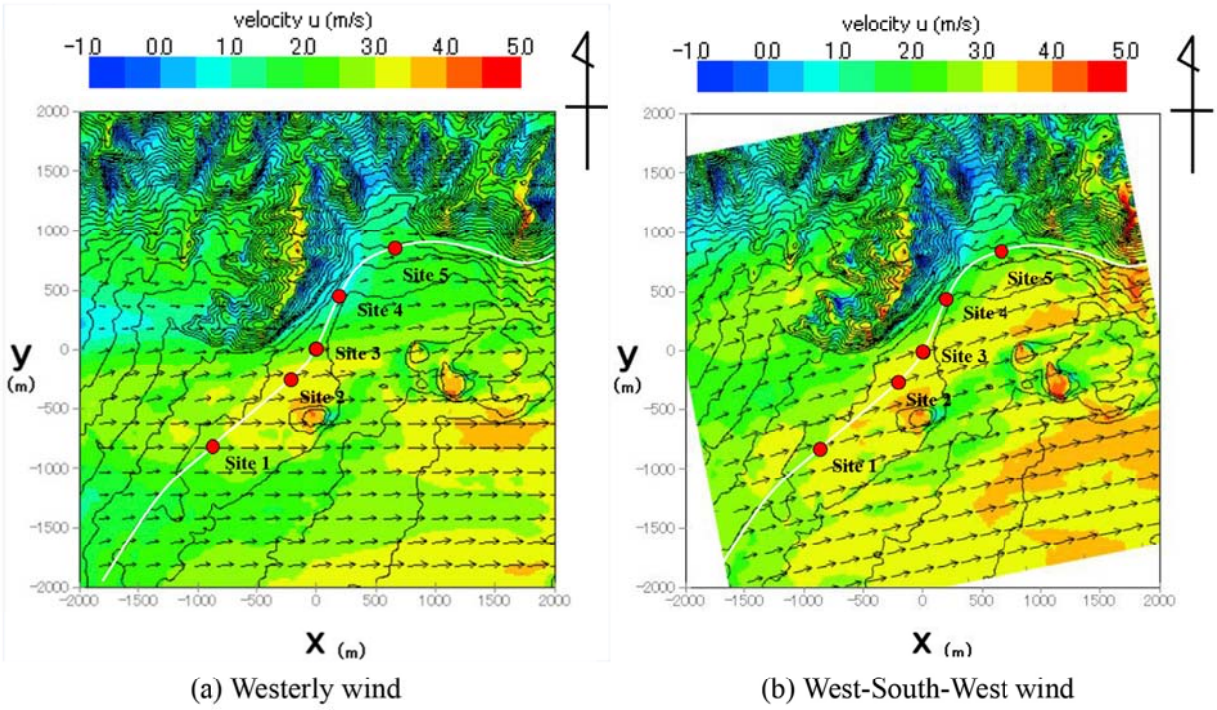

Fig. 5. Predicted velocity vector and wind speed contour in prevailing wind directions.

control section. The elevation contour of the terrain is shown in Fig. 4(a). There is a flat terrain region in south-east area and in the mountain region in north-west area. Surface roughness is shown in Fig. 4(b). There are two lines of high surface roughness at south-west area in the domain and these lines consist of viaducts of Tohoku Highway and Tohoku Shinkansen. Westerly wind at site 1 can be weakened by the wakes of these viaducts, although the terrain around the site 1 is almost flat. Site 4 and site 5 are close to east side of a peninsula like mountain and westerly wind at these sites can be weakened by this mountain. On the other hand, the westerly wind can be strengthened at site 2 and site 3 due to the effect of the mountain.

Predicted velocity vector and wind speed contour are shown in Fig. 5 for the Westerly and West-South-West winds, which are prevailing winds in this area. In this simulation, the wind speed at the upper boundary is set as 10 m/s. Wind directions near surface are not changed from the wind directions at the inlet in south part of the target area in both cases as shown in Fig. 5. The wind speeds at site 4 and site 5 located behind the peninsula like mountains decrease due to the wake of the mountain. As the wind direction changes from West to West-South-West, the wind speeds at site 2 and site 3 increase due to the effect of the mountain and the wind speed at site 1 decreases due to the effects of the viaducts of Tohoku Highway and Tohoku Shinkansen.

2.3. *Validation of predicted maximum wind speed using field measurement*

The wind speed ratio, S_{pr}, and the change in wind direction, D_{pr}, between the prediction sites and the reference site can be expressed by

$$S_{pr} = u_p / u_r \tag{13}$$

$$D_{pr} = \theta_p - \theta_r \tag{14}$$

where, u_r and θ_r are measured mean wind speed and wind direction at the reference site. u_p and θ_p are mean wind speed and wind direction at the prediction site obtained by the linear interpolation based on the numerical simulation results as follows:

$$u_p = u_{p,i} + a(u_{p,i} - u_{p,i+1}) \tag{15}$$

$$\theta_p = \theta_{p,i} + a(\theta_{p,i} - \theta_{p,i+1}) \tag{16}$$

where $u_{p,i}$, $u_{p,i+1}$, $\theta_{p,i}$, and $\theta_{p,i+1}$ are wind speeds and wind directions obtained by the numerical simulation for inlet flow direction sectors, i and $i+1$ at a prediction site. The inlet flow direction sector i is solved from wind directions at reference sites as

$$\theta_r \in (\theta_{r,i}, \theta_{r,i+1}) \tag{17}$$

where $\theta_{r,i}$ and $\theta_{r,i+1}$ are wind directions obtained by the numerical simulation for the inlet flow direction sectors, i and $i+1$ at the reference site.

A proportional coefficient a is assumed as a constant value obtained by

$$a = \frac{\theta_r - \theta_{r,i}}{\theta_{r,i+1} - \theta_{r,i}} \tag{18}$$

The wind speed ratios obtained by the proposed method and observed by the measurement at five sites against site 3 are shown in Fig. 6.

In all cases shown in Fig. 6, the wind speed ratios at site 1, site 4, and site 5 are small, and the ratios at site 2 depend on the wind direction at site 3. In case 1, observed maximum instantaneous wind speed and wind direction at site 3 are 31.9 m/s and west-south-west respectively. In this case, the predicted wind ratio at site 1, site 2, and site 4 show favorable agreement with measured those, while the predicted wind ratio at site 5 is overestimated compared with the measurement due to the wake of the mountains at the north-west side of site 5. However, the effect of the prediction error at low wind speed is small, because the train regulation is issued only at high wind speed. In case 2, the observed maximum instantaneous wind speed and wind direction at site 3 are 31.1 m/s and south-west respectively. The wind speed ratios are slightly overestimated at site 1, site 4, and site 5. The predicted wind speed ratios at these sites are under 0.4 and are low enough to the regulation wind speed. In case 3, the observed maximum instantaneous wind speed and wind direction at site 3 are 31.1 m/s and west respectively. In this case, the wind speed ratios at most sites are well reproduced by the numerical simulation except for site 1. In case 4, the observed maximum instantaneous wind speed and wind direction at site 3 are 29.9 m/s and west respectively. The wind speed ratios are well predicted by the numerical simulation at most sites, although the ratio at site 4 is slightly underestimated.

Fig. 7 shows time series of one minutes maximum wind speed predicted by the proposed method and observed by the measurement at site 2 and site 4 on 25th of January 2005. The predicted winds by the proposed method show good agreement with the measurements. Fig. 8 shows annual frequency distribution of maximum wind at site 2 and site

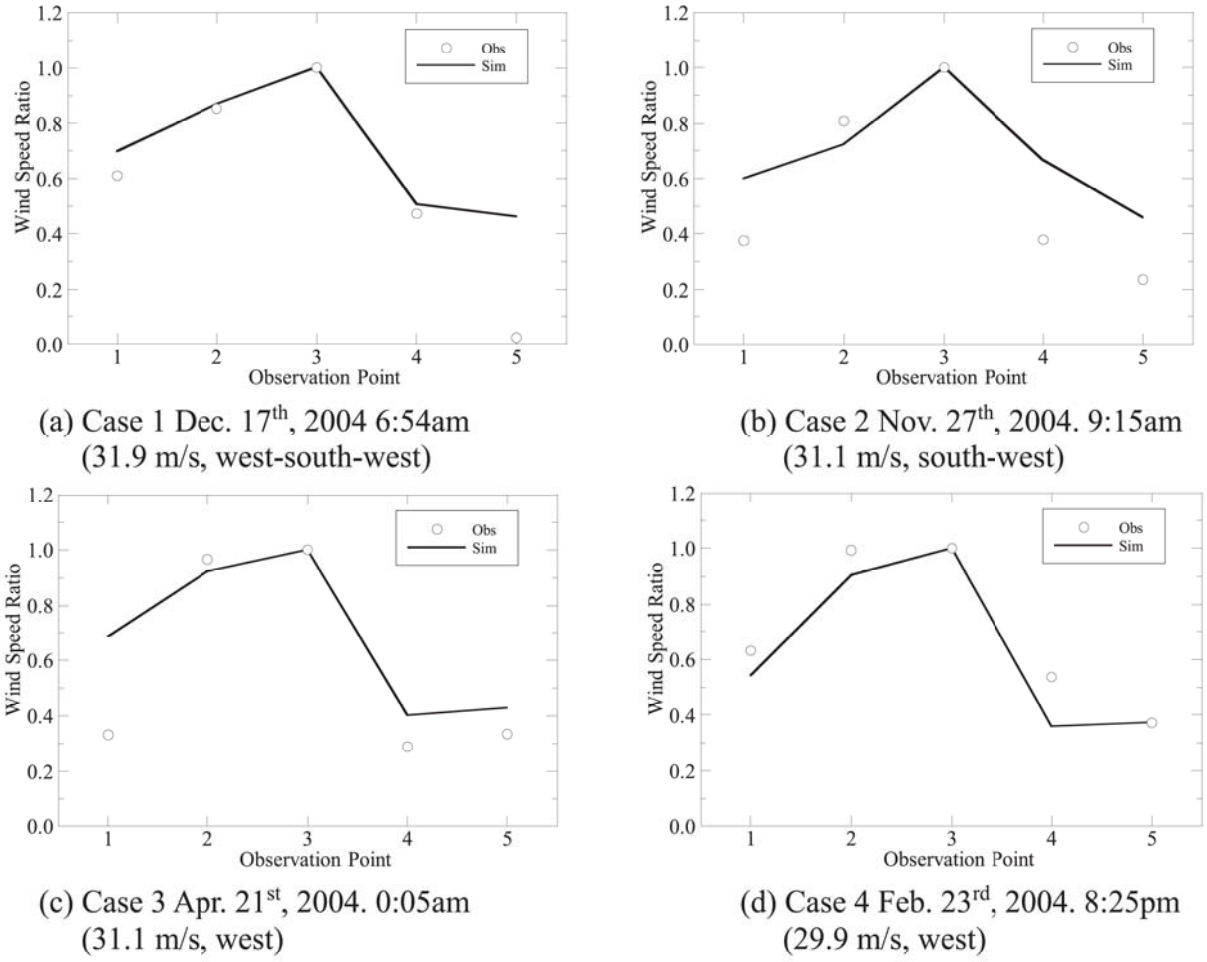

Fig. 6. Comparison of predicted and observed wind speed ratios (Maximum instantaneous wind speed and wind direction at site 3).

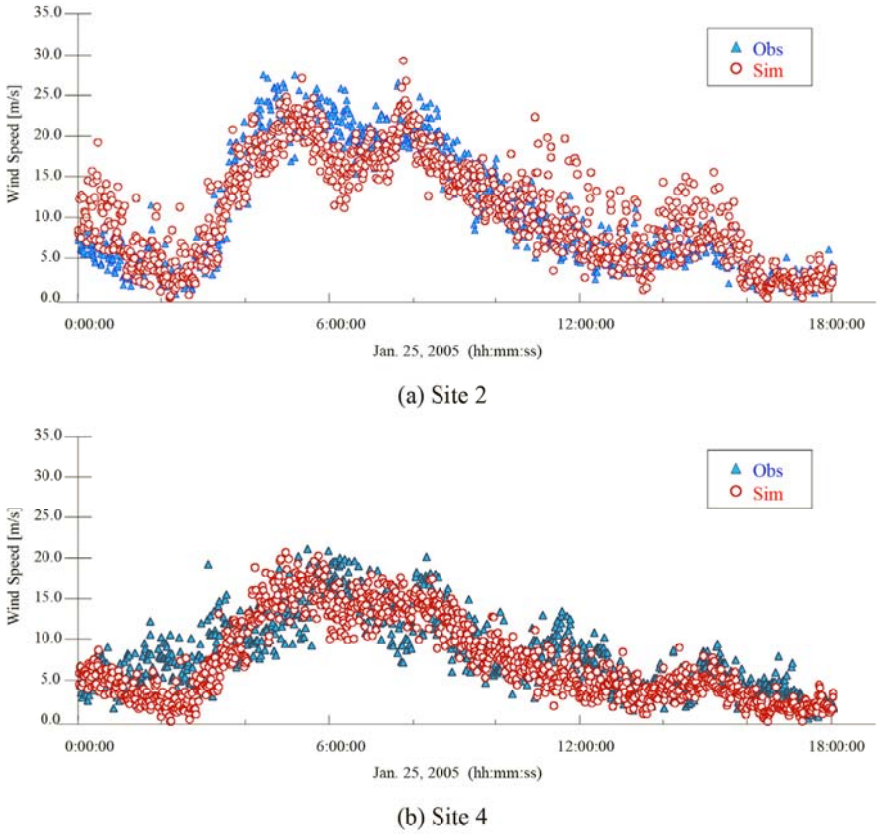

Fig. 7. Comparison of predicted and observed time series of maximum wind speed in one minute.

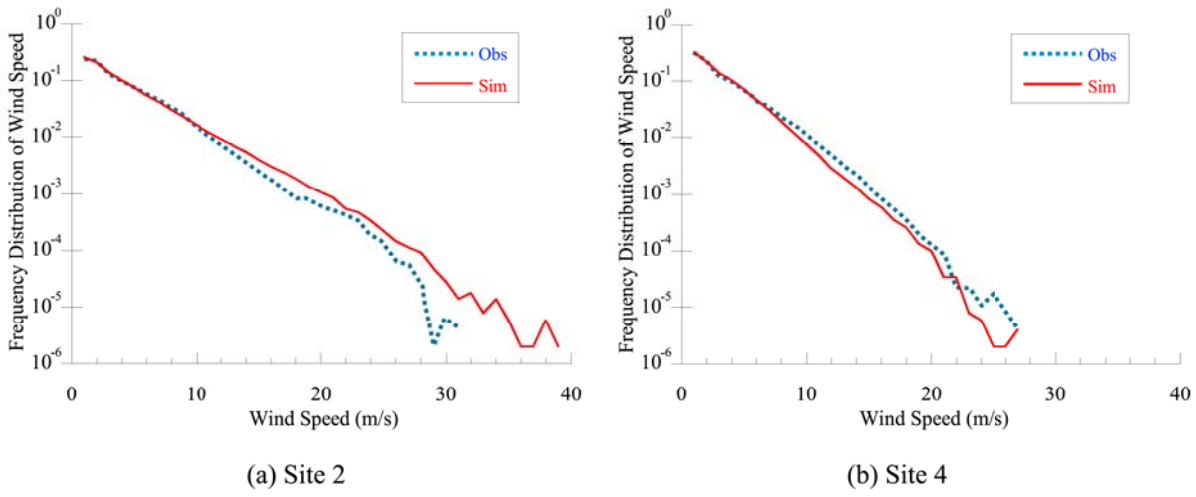

Fig. 8. Comparison of predicted and observed frequency distribution of one minute maximum wind speed.

4 obtained by the proposed method and by the measurement. The predicted annual frequency distributions by the proposed method agree well with the measurement.

3. Prediction for frequency of exceedance of strong crosswind in a control section for train operation

To take efficient countermeasures for strong crosswind, the frequency of exceedance of strong crosswind over the wind speed for regulation at any sites in the control section should be predicted accurately.

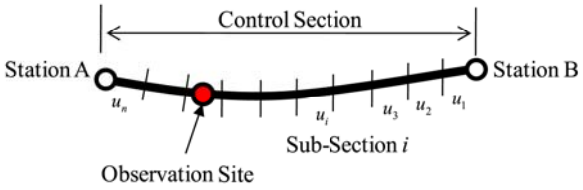

Fig. 9. Definition of sub-sections in a control section.

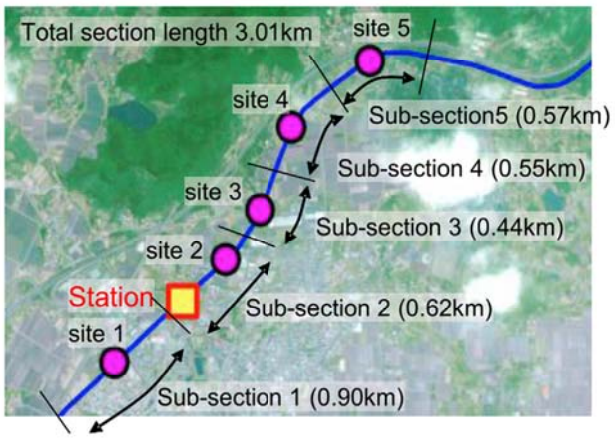

Fig. 10. Control section consists of sub-sections with measurement sites.

In most cases in Japan, the frequency of exceedance is estimated from measured wind speed at one anemometer installed in the control section, assuming that the measured wind speed can represent the winds blowing in the whole control section. Although the frequency of exceedance can be easily estimated by the recorded wind speed at only one site, strong wind events that occur at the site other than the measurement site cannot be included.

In Europe (Matschke et al., 2000; Cléon et al., 2002), a prediction method in which the control section is divided into number of sub-sections is proposed to take account of wind-speed variations due to local terrain in the control section. The strong wind represents in each sub-section can be estimated by measured wind speed, and the wind speed ratio and the change in wind direction from the measurement site to the each sub-section obtained by the numerical simulation. In the method, it is assumed that there is no correlation between the strong winds in sub-sections. By this method, all strong wind events occur in all sub-sections can be taken into account, but the frequency of exceedance of strong crosswind in the control section may be overestimated if the strong crosswind in different sub-sections correlated each other.

In this study, the prediction method that takes account of the correlation of strong wind in different sub-sections is proposed to estimate the frequency of exceedance of the strong crosswind accurately. The prediction results by the proposed method and the conventional methods used in Japan and in Europe are compared with the measurement to evaluate the accuracy of these methods and to clarify disadvantage of the conventional methods.

3.1. Prediction for frequency of exceedance of strong crosswind by time series based method

In this section, the prediction method for the frequency of exceedance of strong crosswinds is proposed to take account of the correlation of strong wind in different sub-sections in a control section. The control section is divided into number of sub-sections as shown in Fig. 9.

Time series maximum wind speeds and wind directions at the representative sites of the sub-sections are obtained by the proposed method outlined in Section 2. Then, the frequency of exceedance of strong crosswind in the control section is obtained by the following equation,

$$P_{nk} = P\left(\max_{i=1,\cdots,n}(\widehat{u}_i) \rangle u^{\text{limit}}\right) \tag{19}$$

where $\widehat{u}_i$ is a maximum wind speed at the representative site of sub-section i, u^{limit} is wind speed for the regulation. P_{nk} is the frequency of exceedance of strong crosswind if the control section k is divided into n sub-sections. In this method, the frequency of exceedance of strong crosswind can be obtained by strictly considering the correlation between the strong winds in different sub-sections, and the time series data of all maximum wind should be preserved. Therefore, this method can be called "Time Series Based Method" (TSM).

The conventional prediction methods for the frequency of exceedance of strong crosswind are also formulized. One is the method by which the frequency is estimated assuming that the recorded wind at one site can represent the wind in the whole control section. In this method, it is assumed that maximum winds in the control section have complete correlation. The frequency of exceedance of strong crosswinds based on this method is described as follows:

$$P_{nk} = P\left(\widehat{u}_{\text{r}} > u^{\text{limit}}\right) = P_{\text{r}} \tag{20}$$

where $\widehat{u}_{\text{r}}$ is a recorded maximum wind speed in the control section and P_{r} is the frequency of exceedance of strong crosswind at the measurement site. The advantage of this method is that the frequency can be estimated from the recorded wind data at only one measurement site, but the disadvantage of this method is that strong wind events that occur at the site other than the measurement site cannot be included and the frequency might be underestimated.

The other is the method which is proposed in Europe as described by the references (Matschke et al., 2000; Cléon et al., 2002). The control section is divided into number of sub-sections, and the wind speed ratio and the change in wind direction from the measurement site to the each sub-section are obtained by the numerical simulation. Assuming that there is no correlation between the strong winds in sub-sections, namely assuming that the strong crosswind in each sub-section is independent, the frequency of exceedance of strong crosswind can be estimated by

$$P_{nk} = 1 - \prod_{i=1}^{n}[1 - P_i] \tag{21}$$

$$P_i = P\left(\widehat{u}_i > u^{\text{limit}}\right) = P\left(u_{\text{r}} \times S_{i\text{r}} \times G_i > u^{\text{limit}}\right) \tag{22}$$

where P_i is the frequency of exceedance of strong crosswind in a sub-section i, $S_{i\text{r}}$ is the wind speed ratio between the reference site and the representative site in the sub-section i and G_i is the gust factor at the representative site in the sub-section i. The advantage of this method is that the frequency can be predicted only by the obtained frequency distributions without storing the time series data of winds in all sub-sections, but the disadvantage of this method is that the frequency can be overestimated due to ignoring the correlation between the strong wind events at different sub-sections.

Since these two methods explained above are based on only statistical data, they can be called "Statistical Data based Method" (SDM).

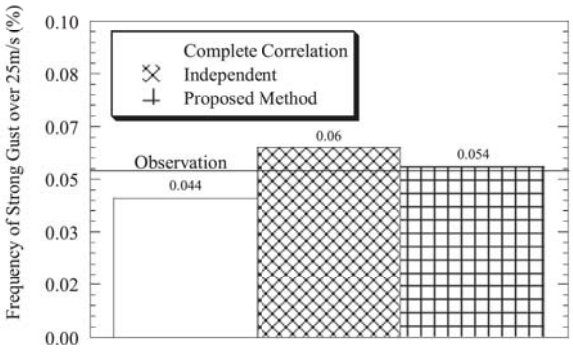

Fig. 11. Frequency of strong crosswind over 25 m/s.

3.2. Validation of prediction for frequency of exceedance of strong crosswind using field measurement

In order to validate the accuracy of the prediction methods, the

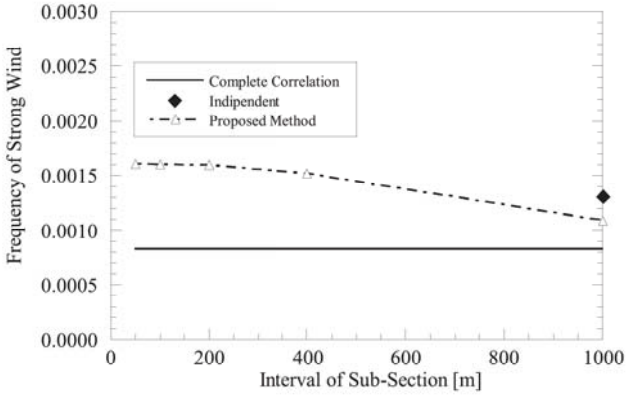

Fig. 12. Frequency of exceedance of strong crosswind with the length of sub-section.

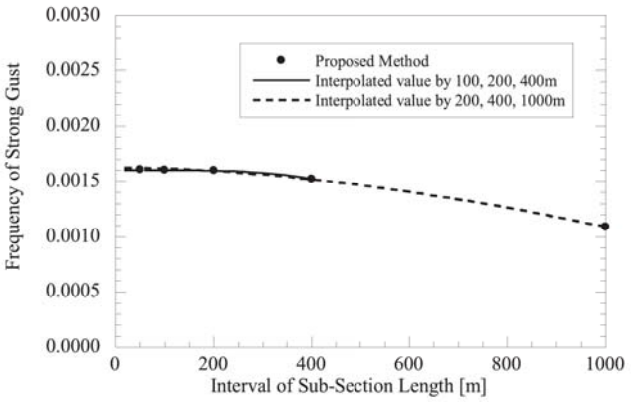

Fig. 13. Comparison of frequencies of strong crosswind over 25 m/s. predicted by proposed method and interpolated by Eq. (23).

frequency of exceedance of strong crosswind in a virtual control section around Fujita station on Tohoku line are predicted by these methods. The virtual control section whose length is about 3 km consists of five sub-sections is shown in Fig. 10. In each sub-section, wind speeds and wind directions were measured for one year from Feb. 2004 to Jan. 2005. Site No.3 is used as the reference site and wind speeds and wind directions at the other sites are estimated by using the prediction methods explained in Section 2.

The frequencies of strong crosswind which exceeds over 25 m/s estimated by three prediction methods are shown in Fig. 11. The line "Observation" shows the frequency obtained from measured data at five sub-sections. The frequency predicted by the proposed method, TSM, agrees well with the observation. On the other hand, the frequency is underestimated by the method "Complete Correlation" which assumes that the measured wind at one site can represent the winds in the whole control section, because the strong wind events that occur at the site other than the measurement site cannot be included. The frequency is overestimated by the method "Independent" which assumes that there is no correlation between the strong crosswind events in sub-sections. In this method, the correlation which exists in reality is ignored, and the strong crosswinds occur in different sub-sections simultaneously are double counted.

The predicted frequencies of strong crosswind over 25 m/s by the proposed methods are shown in Fig. 12, if the length of sub-section is changed from 50 m to 1000 m in a virtual control section around Fujita station whose length is about 6 km. The predicted frequencies obtained by two conventional methods are also shown in Fig. 12. The predicted frequency by the method "Complete Correlation" used in Japan is shown as a straight line. The predicted frequency by the method "Independent" proposed in Europe is shown for the case with the sub-section length of 1000 m, because the sub-section length seems to be set over 1000 m in Europe. All predicted strong crosswind frequencies are shown in Table 2. The predicted frequency by the proposed method tends to be saturated to a certain value and the dependency of the result to the sub-section length decreases as the length decreases. On the other hand, the predicted frequency by the method, "Complete Correlation", is constant and low because this method underestimates the frequency. The predicted frequency for the sub-section length of 1000 m by the method, "Independent", seems to be reasonable, but it can extremely increase if the length of the sub-section decreases. The length of the sub-section should be short if terrain is complex as Japan, and the "Independent" method cannot be applied.

The frequency of exceedance of strong crosswind is expressed as a function of the sub-section length r as follows;

$$P_{nk} = C_1 r^{C_2} + C_3 \tag{23}$$

where C_1, C_2 and C_3 are identified from three frequencies obtained by different sub-section lengths. The independent frequency on the sub-section length is the frequency when the sub-section length is zero, and equals C_3. The parameters of the equation identified from the frequencies obtained by two sets of the sub-section lengths, 100 m, 200 m, and 400 m, and 200 m, 400 m, and 1000 m, are shown in Table 3. The frequencies of exceedance of strong crosswind obtained by Eq. (23) for two sets of sub-section lengths are compared in Fig. 13. The values of C_3 identified by the two sets of the sub-section lengths are 1.60×10^{-3} and

Table 2
Predicted strong crosswind frequencies by conventional and proposed methods (Prediction errors comparing with the independent frequency on the sub-section length 1.60×10^{-3}).

Length of Sub-Section [m]	Complete Correlation	Independent of Each Sub-Section	Considering Correlation to Different Sub-Section (Proposed Method)
50	8.18×10^{-4}		1.58×10^{-3} (−1.47%)
100	(-49.14%)		1.57×10^{-3} (−1.66%)
200			1.57×10^{-3} (−1.96%)
400			1.49×10^{-3} (−6.63%)
1000		1.30×10^{-3} (−18.16%)	1.07×10^{-3} (−32.94%)

Table 3
List of coefficients in Eq. (23)

	Length of Sub-Section [m]	
	100, 200, 400	200, 400, 1000
C_1	-4.74×10^{-15}	-3.04×10^{-9}
C_2	3.93	1.75
C_3	1.60×10^{-3}	1.63×10^{-3}

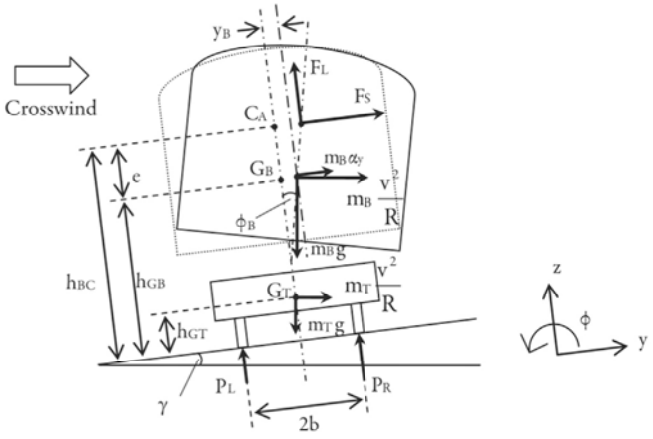

Fig. 14. Forces acting on a train with crosswind (Hibino et al., 2011).

1.63×10^{-3} and the difference of them is sufficiently small.

Comparing with the value of C_3, 1.60×10^{-3}, the prediction errors by three methods in different sub-section lengths can be obtained as shown in Table 2. By the method "Complete Correlation", the prediction error is −49.14% and the frequency is underestimated. By the method "Independent", the prediction error for the sub-section length of 1000 m is −18.16% and it is can be extremely increased as the sub-section length decreases. By the proposed method, the absolute value of the prediction error is less than 2.00% if the length of sub-section is less than 200 m. The frequency of exceedance of strong crosswind can be obtained accurately by setting the length of sub-section about 200 m for the control section selected in this study.

4. Effect of countermeasures for strong crosswind

In this section, a prediction method for the frequency of exceedance of strong crosswind which causes train overturning is proposed, and the effects of countermeasures for strong crosswind, such as reduction of train speed, considering wind direction, and installation of windbreaks, are evaluated quantitatively by the proposed method.

4.1. Calculation of critical wind speed of train overturning

When a crosswind acts on a train, lateral and rolling displacement occur at the train due to the crosswind as described by the references (Hibino et al., 2011; EN 14067-6, 2010; Cheli et al., 2012; Baker, 2013). If the wind speed increases, the displacement increases and weight at the contact point between wheel and rail at windward side, which is called as wheel load, decreases. The overturning of the train starts when the wheel load at the windward side becomes zero. The wind speed when the wheel load at the windward side is zero is called as critical wind speed of train overturning.

A static analysis method of the critical wind speed of train overturning, in which the effect of vehicle suspension and relative wind speed generated by the train running can be taken into account, was proposed by Hibino et al. (Hibino et al., 2011). In the static analysis, gravity acting on a vehicle and bogies, the aerodynamic forces, the unbalanced centrifugal force on a curve, and the lateral acceleration of the vehicle due to track irregularity are considered. The situation that a vehicle is subjected to the crosswind from inside of a curve is shown in Fig. 14, where C_A is the center of wind pressure, G_B is the center of gravity of the vehicle, G_T is the center of gravity of the bogie and γ is cant angle.

The equilibrium of moment at the contact point of wheel and rail at the leeward side is:

$$P_L G = m_B g\left(\frac{G}{2} - y_B\right) + m_T g\frac{G}{2} - F_L\left(\frac{G}{2} - y_B + e\phi_B\right) - h_{BC}F_S - h_{GB}m_B\alpha_u - h_{GT}m_T\alpha_u - h_{GB}m_B\alpha_y \quad (24)$$

where P_L is the wheel load at windward side, $G = 2b$ is the interval of two contact points of the wheels and the rails at windward and leeward sides, m_B is the half mass of the vehicle, m_T is the mass of the bogie, g is the acceleration due to the gravity, y_B is the lateral displacement at the center of gravity of the vehicle, ϕ_B is the rolling angle displacement of the vehicle, h_{BC} is the height of the center of wind pressure of the vehicle, h_{GB} is the height of the center of gravity of the vehicle, e is the distance between the center of gravity and the center of wind pressure of the vehicle, h_{GT} is the height of the center of gravity of the bogie, $\alpha_u = v^2/R$ is unbalanced centrifugal acceleration, v is running speed, R is curve radius and α_y is lateral acceleration of the vehicle. F_S and F_L are the side and the lift forces by the crosswind. The first term and the second term of the right side of Eq. (24) are the moment generated by the gravity applied to the car body and the bogie, respectively. The third and the forth term are both the moment generated by the aerodynamic forces. The fifth and the sixth term are also the moment generated by the unbalanced centrifugal force, and then the seventh term is the moment generated by the force by the lateral acceleration. The critical wind speed of train overturning is the wind speed when $P_L = 0$. F_S, F_L and h_{BC} are described as follows:

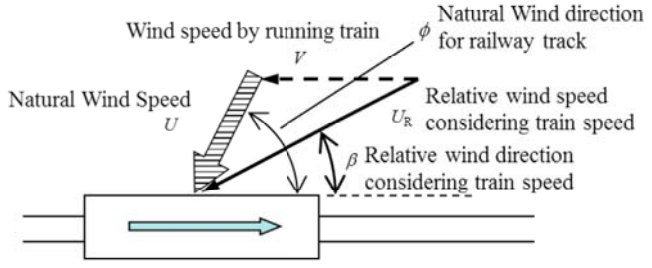

Fig. 15. Definition of relative wind direction considering train speed.

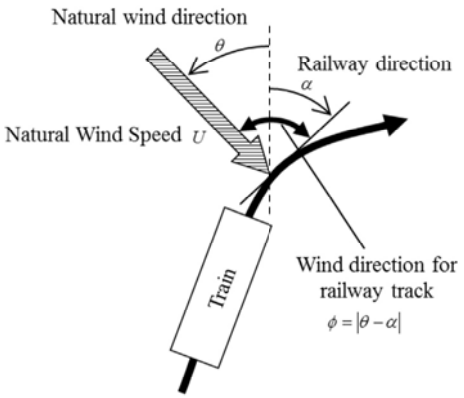

Fig. 16. Definition of relative wind direction for railway.

$$F_S = \frac{1}{2}C_S\rho U_R^2 S_A \quad (25)$$

$$F_L = \frac{1}{2}C_L\rho U_R^2 S_A \quad (26)$$

$$h_{BC} = h_{B1} + \frac{C_{MR}}{C_S}h_{B2} \quad (27)$$

where ρ is the air density and S_A is the lateral area of the vehicle. h_{B1} and h_{B2} are the height of the center of the car body and the height of the car body respectively. C_S is the side force coefficient, C_L is the left force coefficient, and C_{MR} is the rolling moment coefficient obtained by the wind tunnel test using the scaled model of vehicle and structures (Suzuki et al., 2003; Suzuki and Hibino, 2016). In the wind tunnel test, the relative wind speed, U_R, and the relative wind direction, β, consist of the natural wind and the running vehicle, are set as shown in Fig. 15. The relative wind speed, U_R, is obtained from the natural wind speed, U, and the speed of the running train, V, as follows:

$$U_R^2 = (U\sin\phi)^2 + (V + U\cos\phi)^2 \quad (28)$$

where ϕ is the natural wind direction for the railway track.

4.2. Validation of frequency of exceedance of strong crosswind

The wind speed for regulation of train operation is set as the wind speed decided from the minimum critical wind speed of train overturning obtained by the method explained in section 4.1. Since the critical wind speed of train overturning is calculated considering not only natural wind speed but also the wind speed generated by the running of the train, the critical wind speed of train overturning can be improved by reducing the train speed. As a countermeasure for the strong crosswind, the train

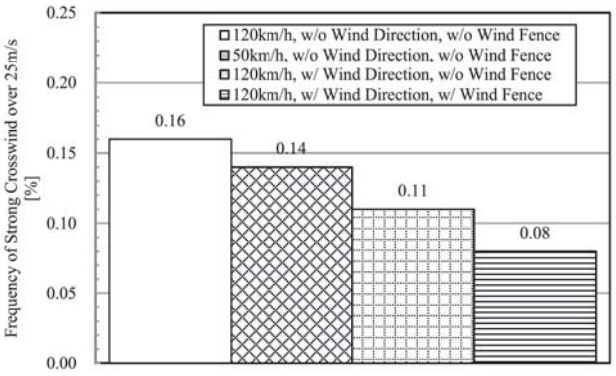

Fig. 17. Frequencies of strong crosswind considering train speed, wind direction, and windbreaks.

speed is reduced or the train is stopped if the observed or predicted wind speed is above the wind speed for regulation.

The critical wind speed of train overturning is defined as a function of the wind direction for the railway track ϕ as shown in Fig. 16. However, if an anemoscope, a sensor of the wind direction, is not installed, the minimum critical wind speed of train overturning should be set as the wind speed for regulation of train operation regardless of the real wind direction, supposing that the wind blows from the worst direction for the overturning. In this case, the frequency of exceedance of strong crosswind which causes train overturning can be overestimated. So, the train operation control can be improved by considering the wind direction.

The train operation control can also be improved by the installation of the windbreaks, by which the aerodynamic forces for the vehicle can be reduced and the critical wind speed of train overturning can be increased.

In this section, a method of the frequency of exceedance of strong crosswind which causes the train overturning is proposed to evaluate the effect of the countermeasures for a strong crosswind, such as reducing the train speed, considering the wind direction, and installation of the windbreaks. The frequency of exceedance of strong crosswind can be obtained as follows:

$$P_{nk} = P\left[\max_{i=1,\cdots,n}\{\widehat{u}_i(t) \times \gamma(V,\phi,C_a)\}\rangle u^{\text{limit}}\right] \tag{29}$$

where u^{limit} is the wind speed for the regulation of train operation, and $\gamma(V,\phi,C_a)$ is the weighting factor of the maximum wind speed related to the countermeasures, such as reducing the train speed, considering the wind direction, and installation of the windbreaks.

$$\gamma(V,\phi,C_a) = \frac{U_c(V_c,\phi_c,C_{ac})}{U_c(V,\phi,C_a)} \tag{30}$$

where the critical wind speed $U_c(V,\phi,C_a)$ is a function of the train speed V, the relative wind direction for the railway ϕ, and the aerodynamic coefficient of the vehicle C_a. V_c, ϕ_c, and C_{ac} are the train speed, the wind direction for the railway track, and the aerodynamic coefficient when the critical wind speed is the lowest.

If any countermeasure is not conducted, V, ϕ, and C_a are equal to V_c, ϕ_c, and C_{ac}, and γ becomes 1. On the other hand, if the wind direction is considered, γ should be less than 1 when the real wind direction is not ϕ_c. Then, the frequency of exceedance of strong crosswind can be reduced. Similarly, if the train speed is reduced or the windbreaks are installed, γ becomes less than 1, and the frequency of exceedance of strong crosswind can be reduced. If there is a limitation of the wind speed U_a for the safety regulated by infrastructures, $U_c(V_c,\phi_c,C_{ac})/U_a$ should be the minimum value of γ.

In order to evaluate the effect of the countermeasures, the frequencies of exceedance of 25 m/s for one year in a virtual control section whose length is 6 km same as section 3.2 are obtained if the countermeasures are conducted. The frequency of exceedance of 25 m/s equals the frequencies of suspension of the train operation for one year.

The frequencies of exceedance of strong crosswind over 25 m/s are shown in Fig. 17. If the train speed reduces from 120 km/h to 50 km/h, the frequency of exceedance of strong crosswind can be reduced from 0.16% to 0.14%, because the critical wind speed can be increased by reducing the train speed. If the direction of strong wind is considered, the frequency of exceedance can be reduced from 0.16% to 0.11%, because the critical wind speed can be increased except for the wind direction ϕ_c at which the critical wind speed is minimum. If the wind direction is considered and the windbreaks are installed, the frequencies of exceedance of strong crosswind can be reduced from 0.16% to 0.08%.

5. Conclusion

In this study, a prediction method for strong wind using onsite measurement and numerical simulation is proposed, and the strong crosswind events in sub-sections are predicted by the proposed method. A time series based method is also proposed to predict the frequency of exceedance of strong crosswind in a control section. The proposed methods are verified by comparisons with the measured wind speed. Following conclusions are obtained.

(1) The prediction method of maximum wind speeds and the wind directions at the prediction sites is proposed. The method consists of the combination of the measurement of mean wind speed and wind direction at reference site and the numerical simulation. Predicted time series of maximum wind speeds and wind directions at any sites along the track by the proposed method show good agreement with the measurement.
(2) The prediction method for the frequency of exceedance of strong crosswind is also proposed with consideration of the correlation of strong wind events in different sub-sections. The accuracy of the proposed method is validated by comparisons with the measurement. Two conventional methods are also clarified. One method with the assumption of the complete correlation of winds in different sub-sections underestimates the frequency, and the other method with the assumption of no correlation of winds in different sub-sections overestimates the frequency.
(3) The effects of countermeasures for strong crosswind, such as reduction of the train speed, considering the wind direction, and installation of windbreaks are evaluated quantitatively. The frequencies of exceedance of strong crosswind over 25 m/s at a 6 km test section decreases from 0.16% to 0.14% when the train speed is reduced from 120 km/h to 50 km/h, and decreases to 0.11% when the wind direction is considered, and further decreases to 0.08% when the windbreak is installed.

References

Avila-Sanches, S., Pindado, S., Lopez-Garcia, O., Sanz-Andres, A., 2014. Wind tunnel analysis of the aerodynamic loads on rolling stock over railway embankments: the effect of shelter windbreaks. Sci. World J. 2014, 1–17.
Baker, C.J., 2013. A framework for the consideration of the effects of the crosswinds on train. J. Wind Eng. Ind. Aerod. 123, 130–142.
Cheli, F., Corradi, R., Tomasini, G., 2012. Crosswind action on rail vehicles: a methodology for estimation of the characteristic wind curves. J. Wind Eng. Ind. Aerod. 104, 248–255.
Cléon, L.M., Parrot, M., Tran-ha, S., 2002. Les vents traversiers sur la LGV Méditerranée. Rev. Gen. Chemins Fer 71–88.
East Japan Railway Company, 2016. CSR Report 2016, p. 40. http://www.jreast.co.jp/e/environment/.
EN 14067-6, 2010. Railway Applications-aerodynamics-part 6, Requirement and Test Procedures for Cross Wind Assessment.
Fujii, T., 1998. Study for the prevention of the overturning of the train in strong wind and countermeasures. JREA 41 (6), 9–12 (in Japanese).
Fujii, M., Fujii, T., Muraishi, H., 1995. History of Railway Operational Regulation under Strong Wind Condition. RTRI report. 9, No.3, pp. 43–44 (in Japanese).
Hibino, Y., Misu, Y., Kurihara, T., Moriyama, A., Shimamura, M., 2011. Study of new methods for train operation control in strong winds. JR EAST Technical Review 19, 31–36.

Imai, T., Fujii, T., Tanemoto, K., Shimamura, T., Maeda, T., Ishida, H., Hibino, Y., 2002. New train regulation method based on wind direction and velocity of natural wind against strong winds. J. Wind Eng. Ind. Aerod. 90, 1601–1610.

Ishihara, T., Hibi, K., 2002. Numerical study of turbulent wake flow behind a three-dimensional steep hill. Wind Struct. 5 (2–4), 317–328.

Ishihara, T., Yamaguchi, A., Fujino, Y., 2003. A nonlinear model MASCOT: development and application. In: Proc. of 2003 European Energy Conference and Exhibition, Madrid.

Ishizaki, H., 1983. Wind profiles, turbulence intensities and gust factors for design in Typhoon-prone regions. J. Wind Eng. Ind. Aerod. 13, 55–66.

Kunieda, M., 1972. Theoretical Study on the Mechanics of Overturn of Railway Rolling Stock. Railway Technical Research Report, No.793, pp. 177–186 (in Japanese).

Liu, Z.Q., Ishihara, T., He, X.H., Niu, H.W., 2016. LES study on the turbulent flow fields over complex terrain covered by vegetation canopy. J. Wind Eng. Ind. Aerod. 155, 60–73.

Liu, Z.Q., Ishihara, T., Tanaka, T., He, X.H., 2016. LES study of turbulent flow fields over a smooth 3-D hill and a smooth 2-D ridge. J. Wind Eng. Ind. Aerod. 153, 1–12.

Matschke, G., Tielkes, T., Deeg, P., Schulte-Werning, B., 2000. Effects of strong cross winds on high-speed trains – a risk assessment approach. In: PSAM 5-Int. Conf. of Probabilistic Safety Assessment and Management, Osaka, Japan.

Matsuda, Y., Shindou, S., Fujii, T., 1997. Countermeasure for strong gust considering wind direction at high embankment and high bridge. In: The Report of Japan Railway Civil Engineering Association. vol. 35. pp. 928–930 (in Japanese).

Misu, Y., Ishihara, T., 2012. Prediction of strong gust frequency in a control section for train operations based on onsite measurement and CFD. J. Japan Association for Wind Engineering 130, 11–24 (in Japanese).

Nakao, N., Amarube Railway Bridge Accident, Failure Knowledge Database, 100 Selected Cases, http://www.sozogaku.com/fkd/en/hfen/HA1000606.pdf.

Suzuki, M., Hibino, Y., 2016. Field tests and wind tunnel tests on aerodynamic characteristics of train/vehicles under crosswind. Quarterly Report of RTRI 57 (1), 55–60.

Suzuki, M., Tanemoto, K., Maeda, T., 2003. Aerodynamic characteristics of train/vehicles under cross winds. J. Wind Eng. Ind. Aerod. 91 (1), 209–218.

Tanemoto, K., Suzuki, M., Saitou, H., Imai, T., 2005. The evaluation of the countermeasures for the strong gust by wind tunnel. Railway Research Review 62 (2), 10–13 (in Japanese).

Yamaguchi, Y., Ishihara, T., Fujino, Y., 2003. Experimental study of the wind flow in a coastal region of Japan. J. Wind Eng. Ind. Aerod. 91, 247–264.